GSA Data Repository 2020078

Rodríguez-Escudero, E., et al., 2020, Pulverized quartz clasts in gouge of the Alhama de Murcia fault (Spain): Evidence for coseismic clast pulverization in a matrix deformed by frictional sliding: Geology, v. 48, p. https://doi.org/10.1130/G47007.1

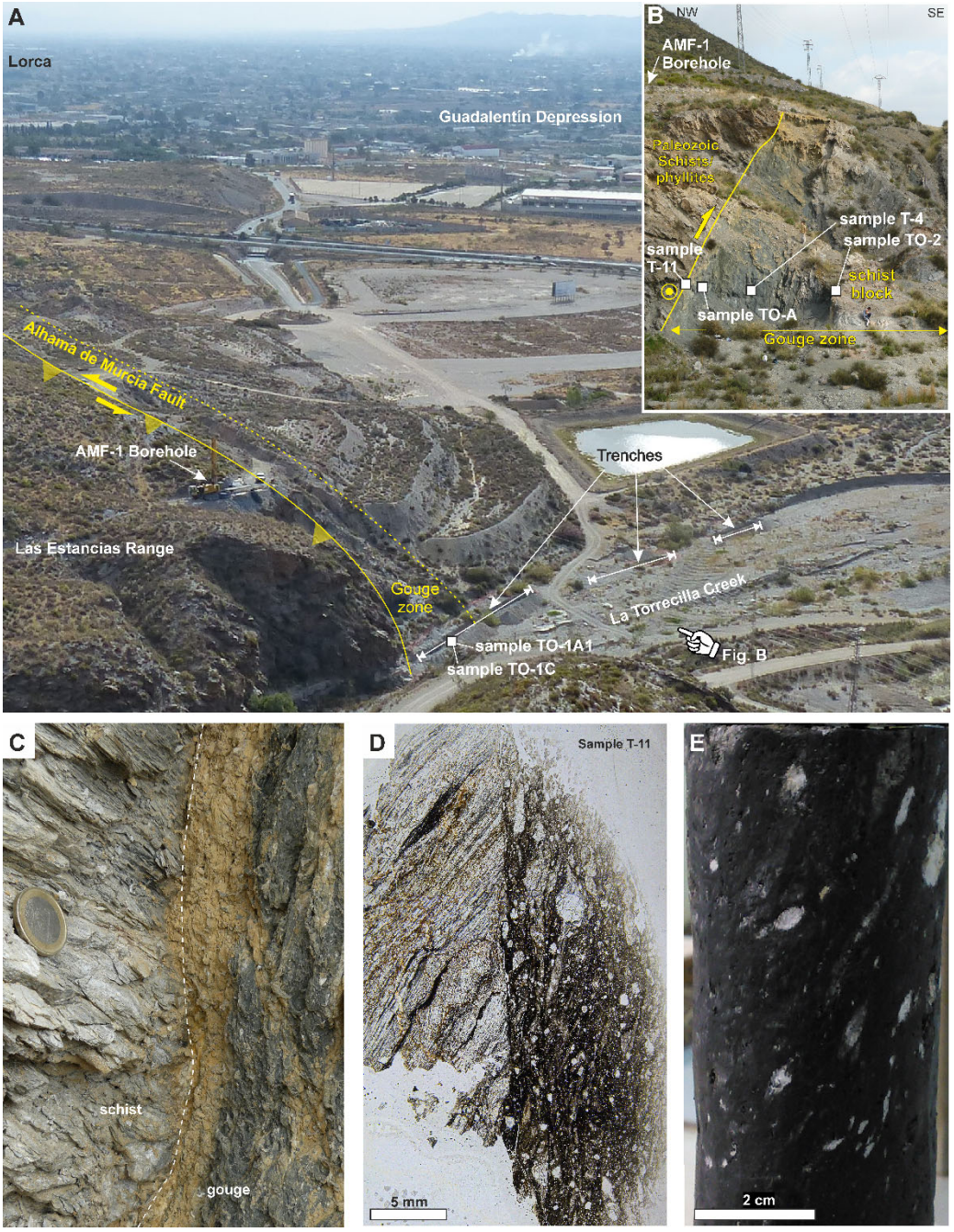

Figure DR1: A, B) General view of the La Torrecilla site and location of the AMF-1 borehole (37.638ºN, 1.747ºW), samples, and trenches excavated across the Alhama de Murcia fault zone (labelled B in A). C, D) Outcrop image and scan thin section of the main fault plane at the contact between the hanging wall rocks (schists/phyllites) and the gouge zone. Sample T-11 shown in D is located in B (37.638ºN, 1.747ºW). E) Sculpted core sample from 135 m depth of foliated gouge with PQCs, resembling mylonite.

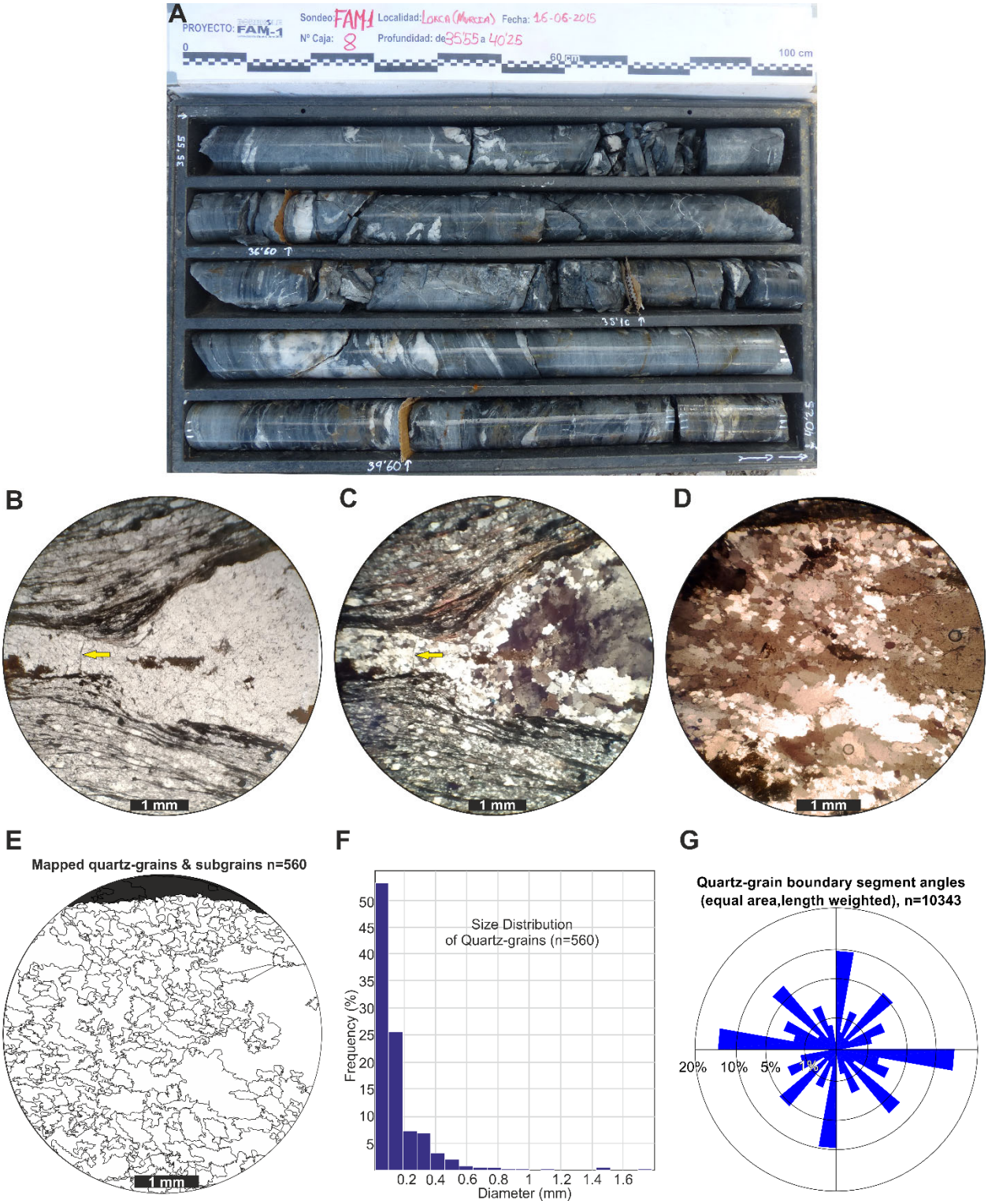

Figure DR2: Structural and textural features of the protolith. A) Drill core image of AMF-1 from 35.55-40.25 m, showing virtually unaltered Paleozoic black schists containing non-brecciated quartz veins. B-C) Representative example of a boudinaged quartz vein in thin section in plane- and cross- polarized light, respectively. Only a few discrete fractures can be distinguished, such

as indicated by arrow. Sample taken in the hanging wall just a few meters from the main fault plane at the La Torrecilla outcrop (37.638ºN. 1.747ºW). D) Cross-polarized view of a quartz vein of the same sample as B, displaying mosaic of quartz as preserved in PQCs. E) Trace map of quartz-grain boundaries from D. F) Histogram showing the grain size distribution of quartz vein determined from E, by using image metrology software. G) Rose diagram displaying the angular distribution of grain boundary segments from E measured using the FracPaQ toolbox.

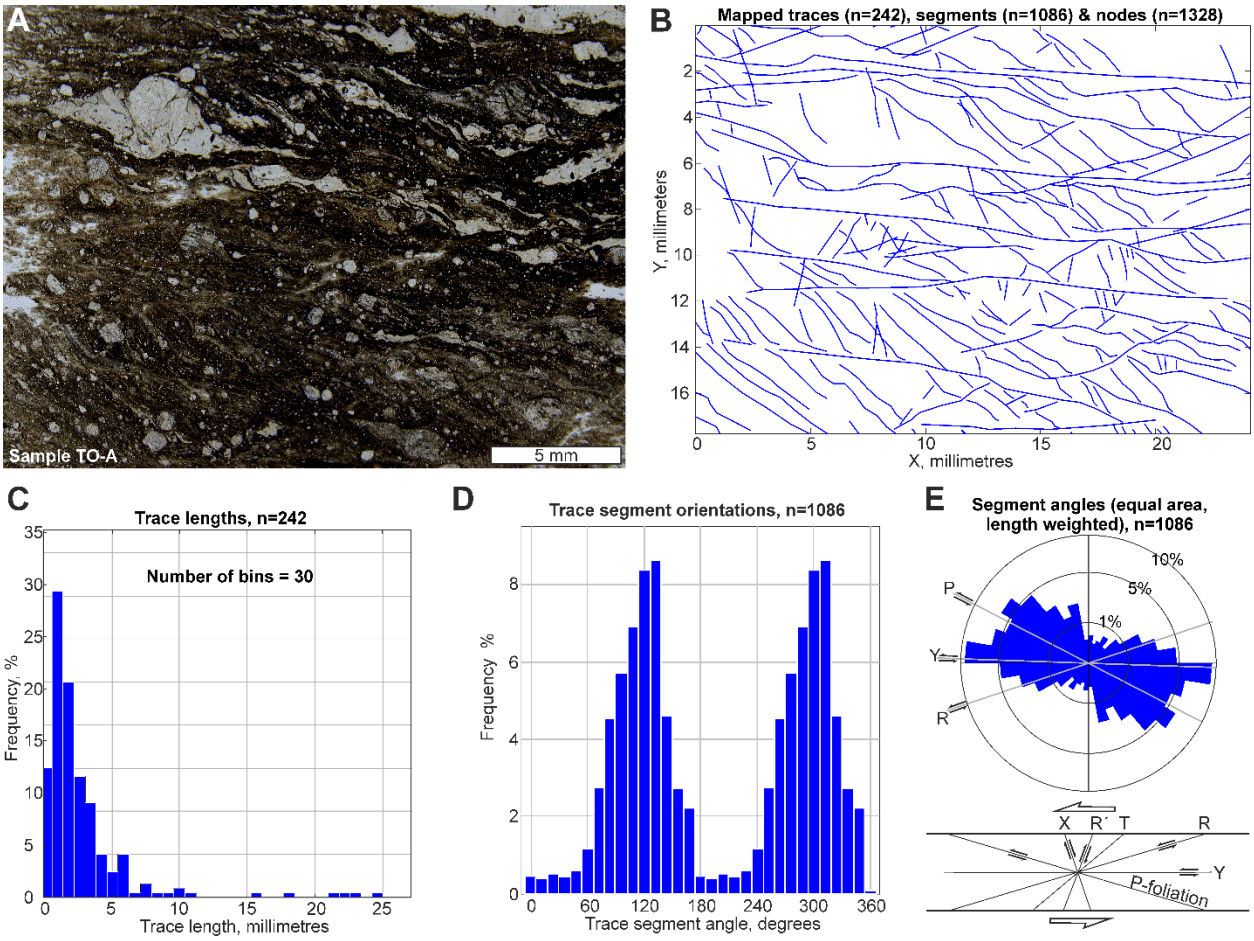

Figure DR3: Quantification of the fracture pattern of the AMF gouge using the FracPaQ toolbox. A) Scan thin section of sample TO-A collected around 1m from the main fault plane at the La Torrecilla outcrop (37.638ºN, 1.747ºW), showing quartz clasts (white) and phyllosilicate/clay rich gouge layers (dark). The sample is shown as Fig. 1C in the main text. See Fig. DR1-B for location. B) Fracture trace map from the thin section of A showing all fracture types including syn- and antithetic sets. Over 200 separate fractures were identified in this 25 x 18 mm area. C) Histogram of fracture trace lengths from B. D-E) Histogram and rose diagram displaying angular distribution and frequency of fracture segments (azimuth interval 10º) with respect to the trace of the AMF, which is parallel to a horizontal reference line. The diagram is arranged to refer to a sinistral sense of shear (top to the left). Note the conjugate fracture pattern corresponding to a Riedel-type fracture pattern as represented at the bottom of the figure.

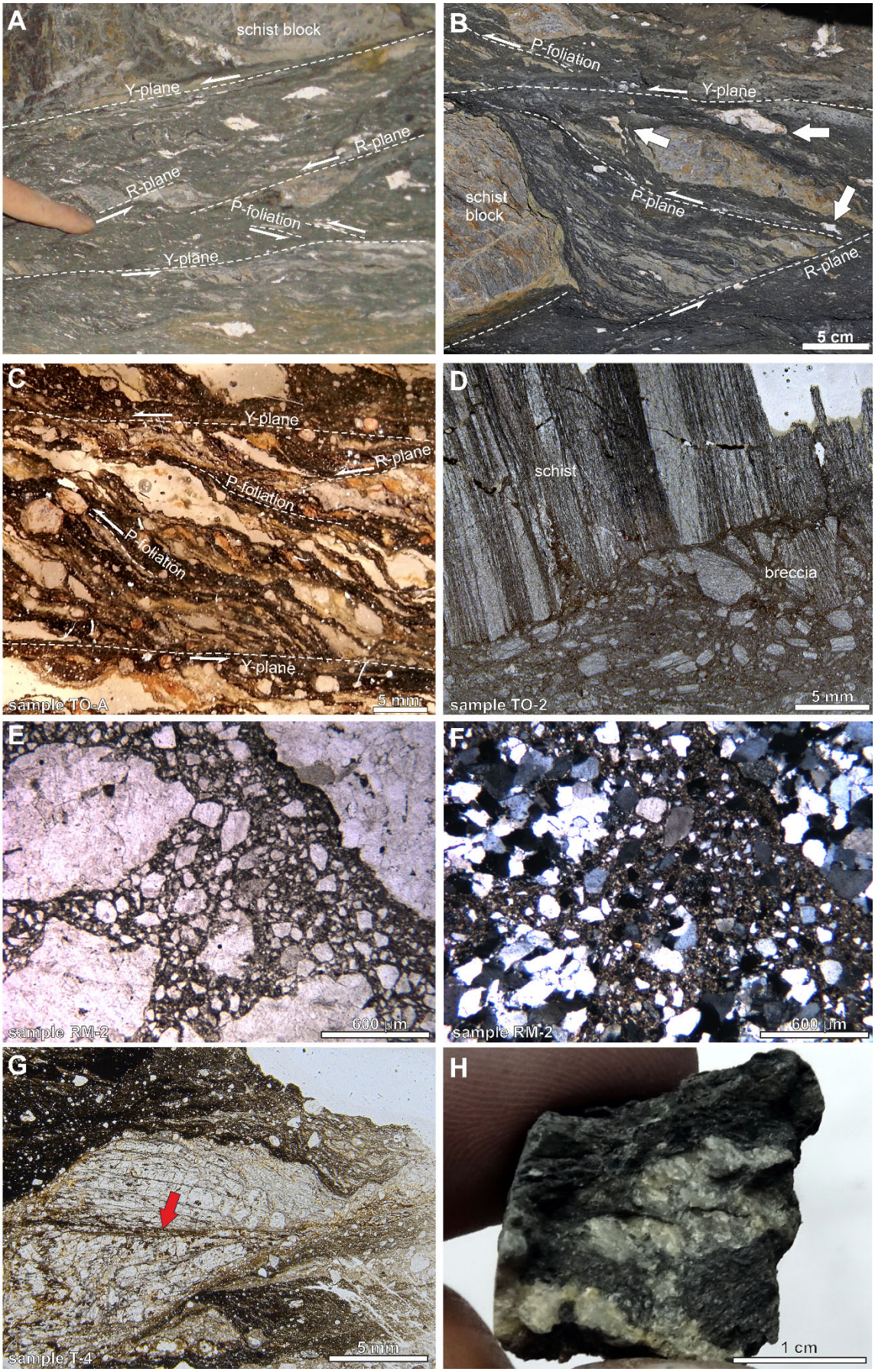
A
schist block
Y-plane
R-plane
R-plane
P-foliation
Y-plane
B
P-foliation
Y-plane
schist
block
P-plane
R-plane
5 cm
C
Y-plane
R-plane
P-foliation
P-foliation
Y-plane
sample TO-A
5 mm
D
schist
breccia
sample TO-2
5 mm
E
sample RM-2
600 µm
F
sample RM-2
600 µm
G
sample T-4
5 mm
H
1 cm

Figure DR4: Structural features of the AMF gouge at meso- and micro-scale. A-B) Close-up of exposures of foliated gouges containing asymmetric pulverized quartz-clasts (white) and schist porphyroclasts (clear gray). P-foliation as well as R- and Y-shears are accentuated in white. C) Scan thin section of sample TO-A showing the gouge fabric, which resembles a mylonite. Oriented, elongated quartz-clasts (white), and comminuted gouge layers (dark) along P-planes, outline a penetrative foliation. P-foliation is dragged into the Y-planes drawing S-C fabrics. D) Detail of contact between schist-block and gouges containing fault breccia (scan thin section of sample TO-2 at 37.638ºN. 1.747ºW; see Fig. DR1-B for location). Towards the gouge (bottom), clasts are oriented and elongated lie within a fine-grained matrix. E-F) Cross- and plane-polarized light section of breccia with non-brecciated quartz-clasts in cataclastic fabric. Sample RM-2 taken in the gouge zone outcropping 1 km north of the La Torrecilla creek (37.646ºN, 1.739ºW). G) Scan thin section of sample T-4 (located in Fig. DR1-B: 37.638ºN, 1.747ºW), showing a shear fracture propagating through schist porphyroclast from the gouge matrix. H) Isoclinal fold formed by quartz fragments alignments in core sample extracted from 136 m depth.

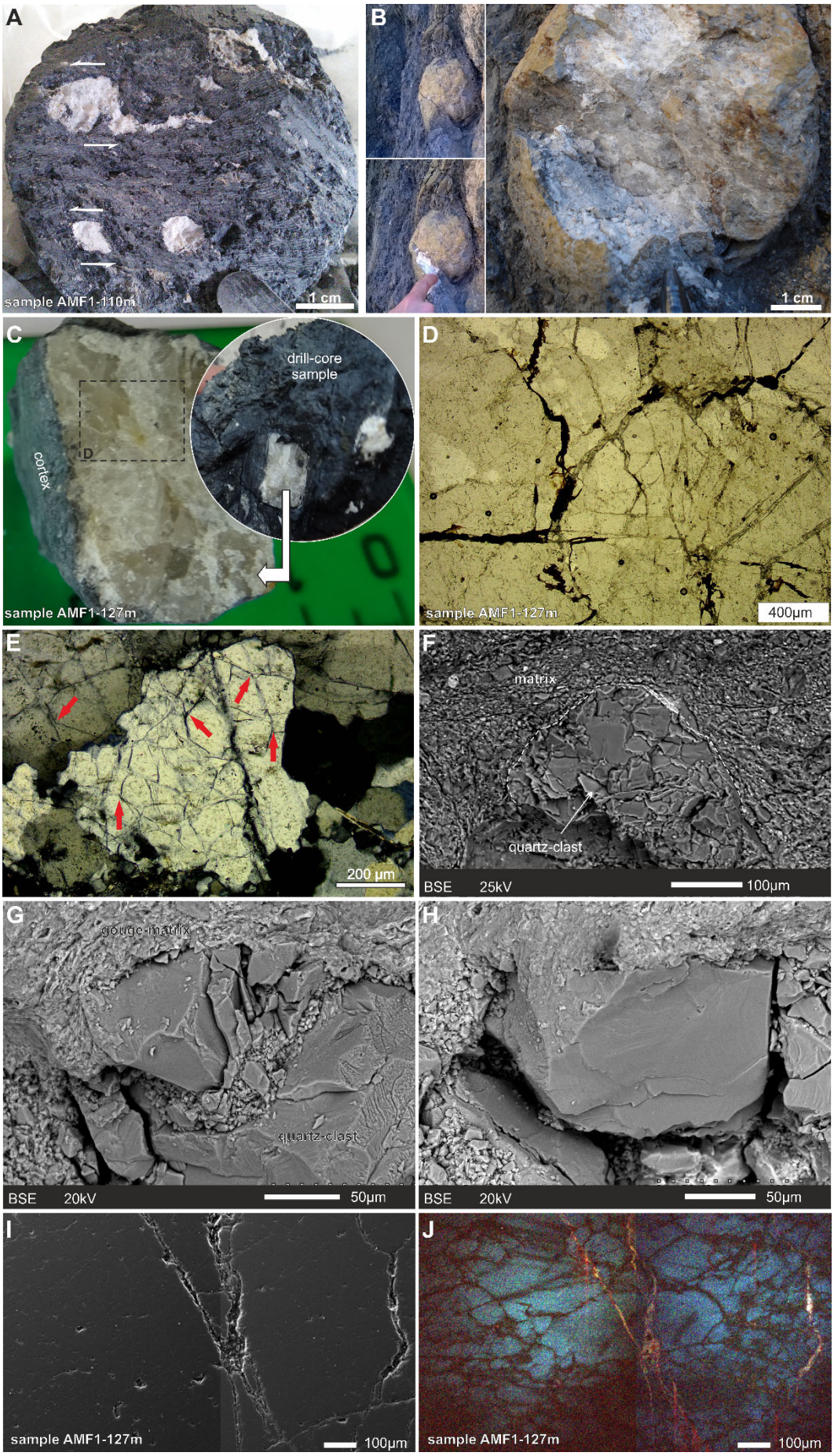
A
sample AMF1-110m
1 cm
B
1 cm
C
drill-core sample
cortex
D
sample AMF1-127m
D
sample AMF1-127m
400µm
E
200 µm
F
matrix
quartz-clast
BSE 25kV
100µm
G
gouge-matrix
quartz-clast
BSE 20kV
50µm
H
BSE 20kV
50µm
I
sample AMF1-127m
100µm
J
sample AMF1-127m
100µm

Figure DR5: Structural features of PQCs from outcrop to SEM. A) Core sample AMF1-110m shows the AMF gouge including typical PQCs with icing sugar texture. A sinistral kinematic is inferred from asymmetric porphyroclasts and tail (indicated with arrows). B) Close up of a rounded quartz-clast, embedded in foliated gouges from the La Torrecilla outcrop (37.638ºN, 1.747ºW), reveals intensive brecciating inside. The clast boundary is not displaced by fractures, suggesting an in-situ shattering mechanism rather than shear. Original crystal texture of quartz is preserved, yet the clast remains incohesive due to the intense micro-fracturing. C) An apparently undisturbed sub-rounded PQC from core sample AMF1-127m shows highly brecciated. Note black (phyllosilicate) cortex surrounds clast suggesting clast rotation. D) Photomicrograph of the highlighted area in C, showing concentric and radial tension fractures that suggests isotropic or quasi-isotropic expansion. E) Photomicrograph of PQC, cross-polarized light, from sample TO-1A1 taken 4 m from the main fault plain (located in Fig. DR1A: 37.638ºN, 1.747ºW), displaying polygonal cracks (some examples arrowed in red) with insignificant grain rotation, to the extent that all fragments going into extinction at the same time exhibiting the original rock fabric. F) Example of SEM image of PQC enclosed within a finer gouge matrix manly composed of phyllosilicates. Note that fracturing in the clast does not propagate through the gouge matrix, and vice versa. Fractures in the clast do not reflect the matrix faults. G) SEM image of sample TO-1 37.638ºN, 1.747ºW) showing a phyllosilicate-rich gouge matrix embedding a PQC affected by open-mode fractures, which reduces the clast to angular micron-size particles. Note that phyllosilicates are aligned around the clast. H) Image of fresh surfaces of quartz particles showing conchoidal fracture. Taken from the same sample as G. I) Mosaic of SEM images of a polished section of the sample shown in C (AMF1-127m), displaying intragranular opening-mode fractures. J) Low resolution cathodoluminescence image of I, revealing an incipient polygonal micro-cracks network with no obvious preferred orientation on quartz segments between major opening-mode fractures.

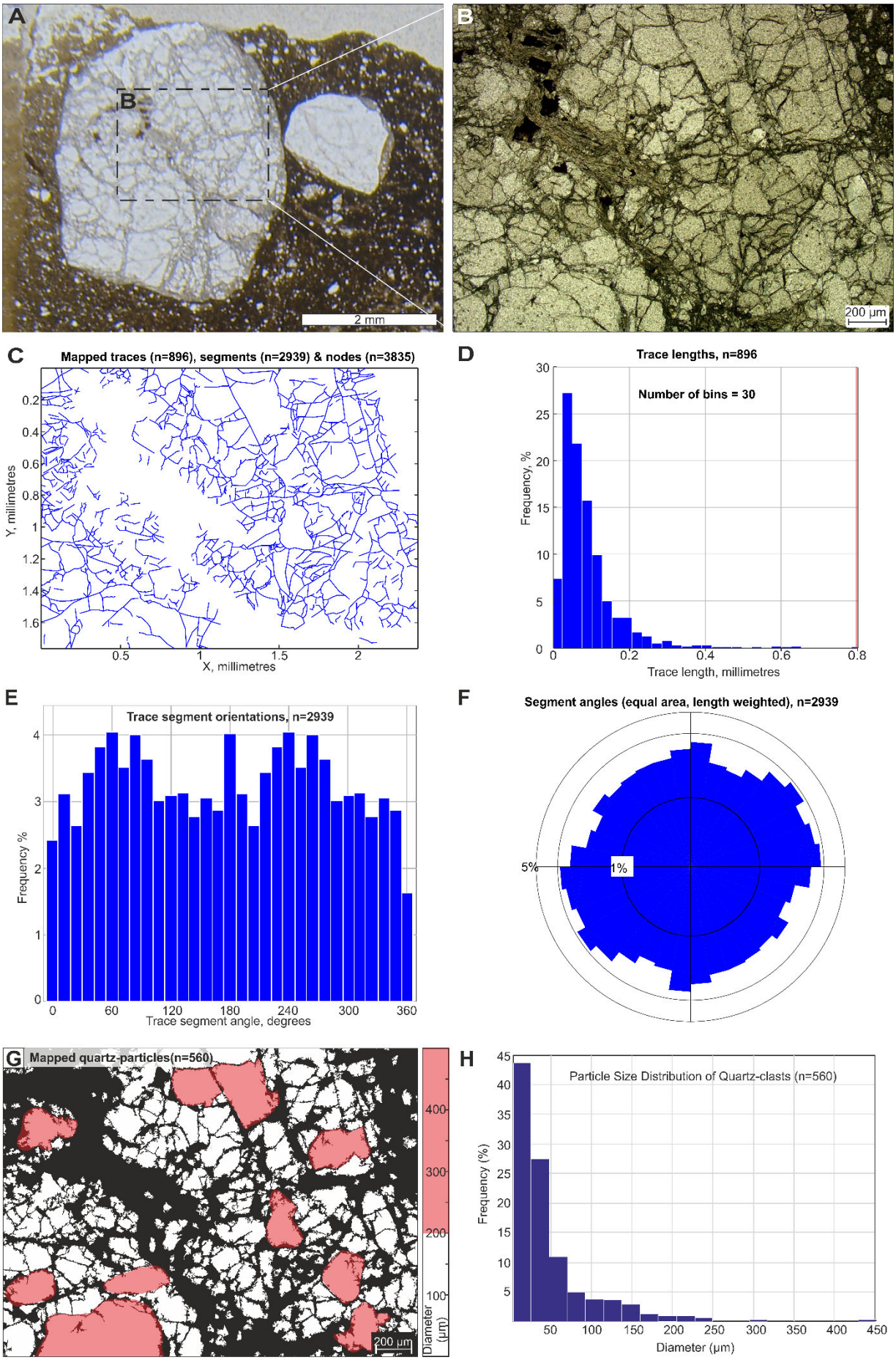
A
B
2 mm
B
200 µm
C
Mapped traces (n=896), segments (n=2939) & nodes (n=3835)
Y, millimetres
X, millimetres
D
Trace lengths, n=896
Number of bins = 30
Frequency, %
Trace length, millimetres
E
Trace segment orientations, n=2939
Frequency %
Trace segment angle, degrees
F
Segment angles (equal area, length weighted), n=2939
5%
1%
G
Mapped quartz-particles(n=560)
200 µm
Diameter (µm)
H
Particle Size Distribution of Quartz-clasts (n=560)
Frequency (%)
Diameter (µm)

Figure DR6: Quantification of fracture pattern and particle size distribution of PQCs. A) Scan thin section of sample TO-1C collected around 4 m from the main fault plane at the La Torrecilla trench (see Fig. DR1-A for location: 37.638ºN, 1.747ºW), showing sub-rounded quartz-clasts in a cataclastic matrix. Shear sense is top to the left. Note that the largest clast is intensely brecciated but shows a net contact with the gouge matrix. Multiple randomly-oriented fractures terminate in the clast-matrix contact, A narrow phyllosilicate cortex surrounds the clast suggesting rigid body rotation, but there is no offset of the clast boundaries or any other evidence of shearing. B) Detail of area marked in A (included as Fig. 2 C in the main text) selected for a quantitative analysis of fracture patterns and particle size distribution, by using the FracPaQ toolbox and image metrology software, respectively. C) Fracture trace map from the area illustrated in B. Over 800 separate fractures were identified in this 2.5 x 1.8 mm area. D) Histogram of fracture trace lengths. E-F) Angles of fracture segments showing a quasi-isotropic distribution, which do not reflect the gouge-matrix fracturing pattern or distribution pattern of the quartz grain boundary segments inherited from the protolith (see Figs. DR2-G and DR3-E for comparison). The rose diagram displays the angular distribution and frequency of fractures with respect to the AMF; the diagram is arranged to refer to a sinistral sense of shearing (top to the left); the trace of the AMF is parallel to a horizontal reference line; azimuth interval 10º. G) Binary image of B used to determine the particle size distribution of PQC, by using image metrology software. Particles larger than 200 µm are highlighted in red. H) Histogram showing the grain size distribution of PQC determined from G. Note that PQC particles are smaller than original quartz grains (see Fig. DR2-F).

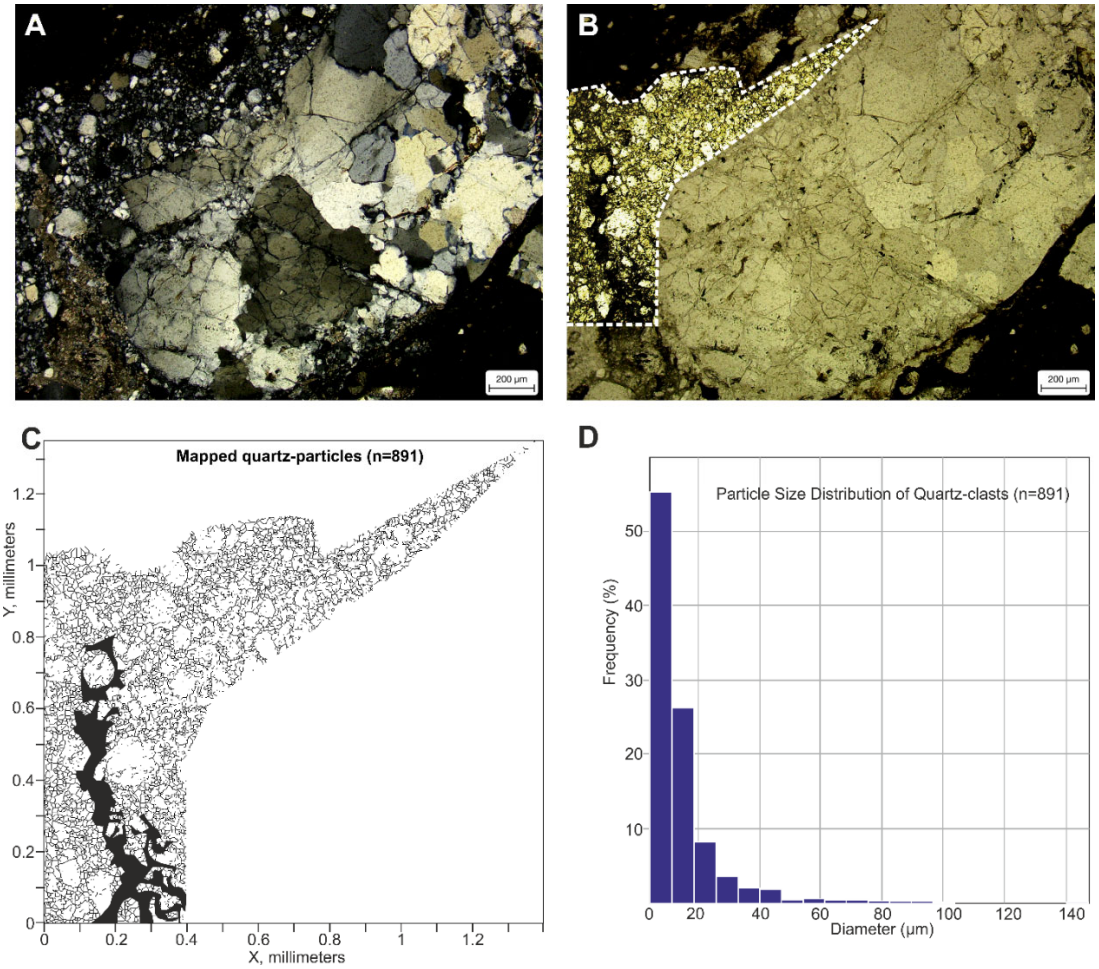

Figure DR7: Grain size analysis of PQC tail. A) Photomicrograph (shown as Fig. 3A in the main text), cross polars, of sample TO-1A1 (37.638ºN, 1.747ºW) partially showing a sigmoidal PQC. Note that the original texture of the protholit is still preserved in the clast-core. In contrast, the finer fragments that extend in the left side as a tail of the clast are randomly extinguished, and there is no continuity between adjacent grains. B) Parallel polars view of A on which a high contrasted image of the selected area used for granulometry analysis, by using image metrology software, is superimposed (dash line). C) Particle-boundary trace map from area marked in B. Over 800 particles were identified in this area. There is no obvious relationship between particle size and distance to the clast-core. D) Histogram showing the particle size distribution determined from C. Note that particle size in the pressure shadow is much smaller than those of clast-core particles (see Fig. DR6-H), suggesting further grinding during migration of particles

from the core to the pressure shadow, due to the gradual “flow” of the gouge-matrix around the PQC.